
Imitrob: Imitation Learning Dataset for Training and Evaluating 6D Object Pose Estimators

J. Sedlar^{1,*}, K. Stepanova^{1,*}, M. Tuna², R. Skoviera¹, J. Behrens¹, G. Sejnova¹,
J. Sivic¹, R. Babuska^{1,3}

¹CIIRC, CTU in Prague, ²MFF, CUNI Bratislava, ³Cognitive Robotics, 3mE, TU Delft

Abstract

This paper introduces a dataset for training and evaluating methods for 6D pose estimation of hand-held tools in task demonstrations captured by a standard RGB camera. Despite the significant progress of 6D pose estimation methods, their performance is usually limited for heavily occluded objects, which is a common case in imitation learning where the object is typically partially occluded by the manipulating hand. Currently, there is a lack of datasets that would enable the development of robust 6D pose estimation methods for these conditions. To overcome this problem, we collect a new dataset (Imitrob) aimed at 6D pose estimation in imitation learning and other applications where a human holds a tool and performs a task. The dataset contains image sequences of three different tools and six manipulation tasks with two camera viewpoints, four human subjects, and left/right hand. Each image is accompanied by an accurate ground truth measurement of the 6D object pose, obtained by the HTC Vive motion tracking device. The use of the dataset is demonstrated by training and evaluating a recent 6D object pose estimation method (DOPE) in various setups. The dataset and code are publicly available at <http://imitrob.ciirc.cvut.cz/imitrobdataset.php>.

1 Introduction

Despite the recent progress [1, 2], 6D object pose estimators are only rarely applied to image sequences capturing manipulation of hand-held objects. However, such a set-up has a huge potential in imitation learning scenarios where expert demonstrations are used to teach robots new tasks (e.g. a human demonstrator manipulating a glue gun to apply glue along specified trajectories). One of the reasons is that there are no datasets and benchmarks that would allow training for such setups. To overcome this problem, we have collected and annotated a real-world hand-held tool manipulation dataset (*Imitrob*) that allows training and evaluating 6D object pose estimators in such conditions.

Acquiring data from videos of humans demonstrating the task has several potential advantages over other approaches such as kinesthetic teaching [3], teleoperation [4], or motion tracking systems with markers on the objects or human body parts [5]. First, such a set-up can provide more detailed information about the interaction of the tool with the environment. Second, it is also much easier for a skilled worker to perform the task in the usual way rather than to demonstrate it by holding a robot arm. Third, such a set-up enables easier transfer to different robotic platforms. Finally, vast amounts of visual data are already available (e.g. instructional videos on YouTube).

However, there are also several critical challenges that need to be addressed. First, we have to deal with the fact that hand-held objects are typically partially occluded by the demonstrator, contain various symmetries, and lack a distinctive texture. These characteristics make training of 6D object pose estimators difficult, and whether their tracking accuracy will be sufficient for the robotic task is a priori unclear. Second, to guarantee a reasonably short setup time (e.g. data collection,

*Both authors contributed equally. E-mail: jiri.sedlar@cvut.cz, karla.stepanova@cvut.cz

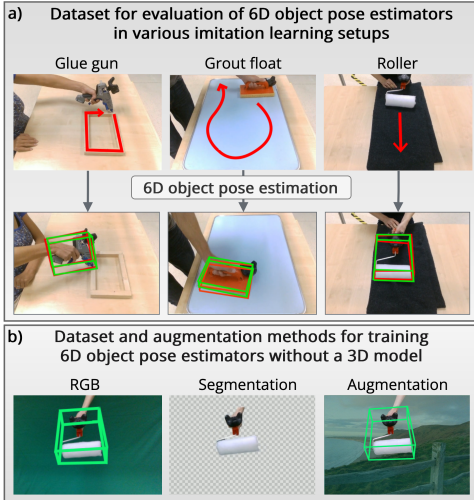


Figure 1: *Imitrob* dataset for 6D object pose estimation of hand-held tools in real-world manipulation tasks in uninstrumented environments. The dataset consists of two components: a) *ImitrobTest* dataset for benchmarking 6D object pose estimation methods, and b) *ImitrobTrain* dataset for training 6D pose estimators without a 3D model of the tool.

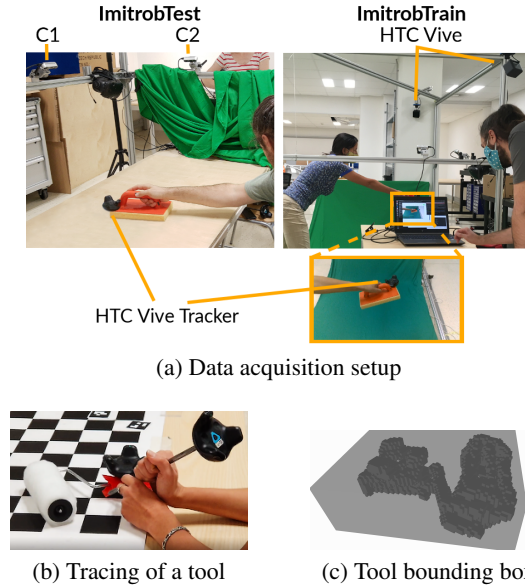


Figure 2: **The experimental setup for collection of *ImitrobTest* and *ImitrobTrain* datasets.** a) The setup consists of RGB-D cameras, HTC Vive light-houses, and a tracker attached to the tool. b) The surface calibration process. c) The resulting voxel grid (dark gray) and bounding box (light gray).

processing, and annotation), the 6D object pose estimator must be trainable on a limited amount of demonstration data. Finally, the 6D pose estimator should preferably work without a 3D model of the tool because current model-based pose estimation methods require high-quality object models, which are difficult to acquire in real-world imitation learning applications.

Thus, the development of data-efficient and occlusion-resistant 6D object pose estimators requires datasets focused on manipulation with hand-held tools, as well as a methodology on how to evaluate the performance with regards to imitation learning tasks, neither of which currently exist. Our paper addresses this problem and provides tools that help to improve the performance of 6D object pose estimation in such challenging cases. We present the following main contributions:

1. We have collected, annotated, and published a real-world hand-held tool manipulation dataset, called *Imitrob* [6] (see Fig. 1). The dataset consists of RGB-D videos with ground truth annotations of the tool 6D poses and bounding boxes. The pose annotations are generated using the HTC Vive motion tracking system, and the bounding boxes are derived from the tracked pose and a tracing-based object surface estimation. The *Imitrob* dataset contains 3 hand-held tools (glue gun, grout float, and roller), manipulated by 4 demonstrators, using left/right hand, and recorded from 2 camera viewpoints. The testing part of the dataset (61 660 images), called *ImitrobTest*, includes videos of six manipulation tasks in realistic environments simulating controlled industrial settings with stable artificial lighting and fixed camera poses, as can be expected in the target use-cases. The training part of the dataset (39 326 images), called *ImitrobTrain*, contains random motion of the tools in front of green background. The *Imitrob* dataset is useful as a benchmark to compare inference algorithms for hand-held object pose estimation in general.
2. We provide a methodology (accompanied by a software package [7]) to collect and ground truth training data for new objects or manipulation tasks with an affordable setup. The methodology can also be used to introduce further variability into the dataset. The data acquisition methodology does not require a CAD model of the tracked tool to obtain the ground truth 6D pose. For application in industrial environments, the methodology requires only simple modifications (e.g. attaching a tracker to the tool), which we regard as an essential component for practical use of imitation learning in real-world set-ups, e.g. in industrial environments.

3. To illustrate how the *Imitrob* dataset can be used to compare the performance of various object pose estimators with respect to various setups, we have trained and evaluated the accuracy of a selected 6D object pose estimator (DOPE [2]).
4. We demonstrate how the generalization capabilities of the 6D object pose estimator can be enhanced by augmentation of the *ImitrobTrain* dataset. For this purpose, we compared several data augmentation techniques; the best performance was achieved by a method that leverages the blending of the original and random background.

All available materials can be downloaded from our project webpage [6].

2 Related Work

In this section, we focus on the current datasets aimed at static 6D object pose estimation and on those that include videos depicting manipulated objects for imitation learning. We also mention the state-of-the-art methods in 6D object pose estimation from RGB and RGB-D images or videos.

6D object pose estimation. Motivated by applications in robotics, 6D object pose estimation has recently attracted significant attention [2, 8, 9]. In the case of richly textured objects, methods based on matching of local invariant features such as SIFT [10] or SURF [11] produce reasonable results, but unfortunately, many hand-held tools are not richly textured. The more complicated 6D estimation of textureless objects can be handled by models based on Convolutional Neural Networks. Methods such as [12, 13] use CNNs to directly regress 6D object pose. In another approach, methods like [14–20] predict the correspondences between the 2D input image and either a 3D model of an object or specific keypoints on an object, which are then used to compute the object 6D pose via the PnP algorithm. The DOPE algorithm [2] is a keypoint matching method that predicts the object’s 3D bounding box vertices and centroid locations in the 2D coordinate system of the input RGB image. This approach was shown to outperform other models like the PoseCNN [12]. There are also more recent methods, such as [1, 14], which estimate the 6D pose based on the alignment of 3D object models with the input images. However, these “render-and-compare” methods require a known 3D model of the object. Obtaining such accurate 3D models quickly is a nontrivial task in real-world imitation learning scenarios. Hence, we choose DOPE [2] as our exemplar 6D pose estimation method as it does not require a 3D model of an object to estimate the pose. Instead, only visual data and reference 6D pose data are needed. DOPE is thus more suitable for imitation learning setup as it only requires the user to record a few short training videos with the hand-held tool.

Datasets for 6D object pose estimation. One of the frequently used static datasets for object pose estimation is Linemod [21], which consists of 15 textureless household objects with annotations and a test set that includes these objects in cluttered scenes. An extended version Linemod-Occluded [22] introduces a more challenging occluded testing scenario. The T-LESS dataset [23] features 30 objects from an industrial environment, which lack an easily discriminative texture and are symmetrical along one or more axes. Another industry-oriented dataset is ITODD [24], but its reference annotations are not available for the test images. The recent YCB-M dataset consists of real-world static scenes recorded using 7 different cameras [25]. In all of the above-mentioned datasets, the objects are static and captured by a camera moving around the object at an approximately constant distance. However, for more realistic real-world 6D object pose estimation, it is beneficial to train the estimators on datasets depicting manipulated objects. Creating such datasets is even more technically challenging. Hence, the existing datasets are small or employ methods that simplify the annotation task [12, 26]. For example, the authors of the YCB-Video dataset [12] avoided full manual annotation by keeping the recorded objects at fixed positions and moving the camera only, leading to a high correlation of the objects’ relative poses throughout the data. Compared to the Linemod or YCB-Video datasets, we focus on specific tasks and tools typical for industrial manufacturing environments. A real human activity RGB dataset focused on task-oriented grasping [27] includes both synthetic and real RGB-D videos of manipulated objects. However, the annotations are mainly focused on the hand joint positions, and only a small proportion of the objects are provided with their meshes and 3D poses. Probably most related to ours is the dataset [28], which consists of three objects recorded with the Kinect sensors. Our dataset differs in the three main aspects. First, we obtain the reference 6D pose from an HTC Vive controller attached to the object, whereas [28] used manual annotation. Second, [28] provides 3 187 images in total, whereas our whole dataset contains more than 100 000 images. Third, [28] lacks variability across several subjects, left and right hand,

different camera views, tasks, or clutter in the scene. Furthermore, [28] expects a known 3D model of the object and thus cannot be used for the training of 3D model-independent estimators. We are unaware of any other 6D object pose estimation video dataset besides ours that would enable the evaluation of trained models for so many different types of generalization, i.e. across different human operators, left-handed and right-handed manipulation, task variations, camera viewpoints, occlusions, and backgrounds. To demonstrate its utility, we measure the impact of each of these challenges on the accuracy of 6D object pose estimation provided by the DOPE algorithm [2].

3 Data acquisition setup

The basic data acquisition setup (see Fig. 2a) consists of a desk with two Intel RealSense D435 RGB-D cameras and an HTC Vive VR set. The data from all sensors are broadcasted as Robot Operating System (ROS [29]) messages and stored in ROS bag files. The cameras produce 848×480 RGB-D images at 60 Hz, and the HTC Vive produces 6D poses at 30 Hz. For the data collection, each task was performed on a table with task-related or clutter objects (see Fig. 3). We recorded the dataset in our laboratory in settings simulating a controlled factory environment with stable artificial lighting and fixed camera poses.

Sensor setup calibration and data synchronization. For the cameras, we estimated the intrinsic parameters and the radial and tangential distortion coefficients from several views of the chessboard calibration pattern using the OpenCV library [30]. The extrinsics were calibrated from a single view of the chessboard pattern. The origin of the chessboard (world) coordinate system O_w was defined in one of the chessboard corners, and the camera poses relative to O_w were estimated by solving the PnP problem in combination with the RANSAC algorithm. To calibrate the HTC Vive coordinate frame O_{htc} (in one of the lighthouses marked as HTC Vive in Fig. 2a) to the chessboard coordinate frame O_w , spherical motion patterns centered at different chessboard corners p_w were recorded using a tracked pointing device (tracker mounted on a pointed metal rod, shown in Fig. 2b). More technical details of the calibration are presented in Appendix A.1. The average deviation (residual r_{avg}) of the acquired center points from the regular chessboard grid pattern (acquired from the cameras) was below 2 mm for all experiments. The HTC Vive pose data were interpolated to calculate the reference object poses for the times when the individual camera images were captured. When the time difference between consecutive HTC Vive frames is longer than 100 ms, the corresponding camera images are discarded to ensure sufficiently accurate ground truth data.

HTC Vive Tracker to Tool Calibration. To be able to provide the reference bounding boxes for the *Imitrob* dataset, we first have to find the bounding boxes of the manipulated objects relative to the tracker. To find the object dimensions relative to the tracker, we traced the tool and tracker surfaces with a tracked pointing device while recording the positions of both trackers (see Fig. 2b). Contour tracing for surface reconstruction was described in [31]. The acquired surface points are filtered (points that are likely not part of the surface are removed), and a voxel grid with the dimensions of the object is created. Finally, we calculate a minimal bounding box aligned with the tracker’s z -axis using the trimesh library [32] while evaluating volumes for different rotations. Fig. 2c visualizes the resulting voxel grid and bounding box for the roller. Note that a small systematic error in the computed bounding boxes should not affect the performance of 6D pose estimators because the training and testing are executed using the same bounding box calibration. The accuracy of the pose annotations is mainly determined by the HTC Vive dynamic accuracy, which was evaluated in [33] as typically around 1 mm. The details of the whole procedure and its accuracy are described in Appendix A.2.

4 Dataset for benchmarking and training 6D object pose estimators

Our *Imitrob* dataset provides annotated videos of manipulation tasks with hand-held tools in a real-world environment. The dataset is designed for benchmarking of 6D object pose estimators applied in industrial tasks, such as imitation learning or object grasping. Imitation learning requires demonstrations of the tool trajectories relative to the object of interest, variety of demonstrators, the use of left and right hand, etc. We took care to represent all these aspects well in the dataset.

The motivation for the tools used in the *Imitrob* dataset, i.e. glue gun, grout float, and roller, comes from actual industrial cases. For instance, glue guns are used in the production of aerospace equip-

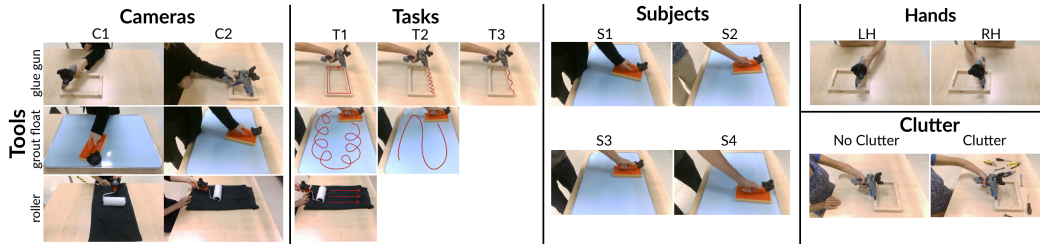


Figure 3: **Overview of the variability of setups provided in our *ImitrobTest* dataset.** **Tools** (rows): glue gun, grout float, and roller. **Cameras**: front (C1) and right hand side (C2), synchronized in the *ImitrobTest* dataset. **Tasks**: frame (T1), dense wave (T2), and sparse wave (T3) for glue gun; round (T1) and sweep (T2) for grout float; press (T1) for roller. **Subjects**: four demonstrators (S1, S2, S3, S4). **Hands**: left (LH) and right (RH) hand. **Clutter**: workspace with only the gluing frame (No Clutter, default) and with other objects on the table (Clutter).

ment for airplanes, including baggage bins, kitchen galleys, trolleys, etc., among many other applications. Due to the large variability in this equipment, a large amount of repetitive manual labor is involved, which is very difficult to replace by robots. Another example is the sealing of plastic foil in car doors, where rollers are used to press the foil against the metal frame on which glue has been applied. In contrast, there is less need for imitation learning for tools such as saws and screwdrivers, which are typically part of specialized robot end-effectors and thus already commonly used in many robotic applications.

We see the following three main usages of the provided dataset and methods: 1) Benchmarking 6D pose estimation methods for hand-held tools in manipulation tasks; 2) Methodology for data acquisition and 6D pose estimator training for new tools and tasks; and 3) Guideline for collecting more extensive datasets and benchmarking 6D object pose estimators on various tasks with hand-held tools, e.g. in imitation learning.

The *Imitrob* dataset consists of two main components: 1) *ImitrobTest* dataset and evaluation metrics for benchmarking 6D object pose estimation methods and 2) *ImitrobTrain* dataset and augmentation methods for training 6D pose estimators that do not require a 3D model of the object. The following sections describe these components in detail. The dataset and methods can be downloaded at [6].

4.1 *ImitrobTest*: Dataset for benchmarking

The *ImitrobTest* dataset (see Fig. 3) provides real-world benchmarking data for 6D object pose estimation in an imitation learning setup. It enables the evaluation of various setup combinations that we typically expect in the case of imitation learning in industrial settings. These variations include the manipulated tool, performed task, camera viewpoint, demonstrating subject, hand used for manipulation, or presence of clutter in the scene. In total, there are 112 different tool/task/camera/hand/demonstrator/clutter combinations in the *ImitrobTest* dataset. Inspired by common trajectory-dependent industrial tasks, we focus on the scenario where the robot is observing a manipulation of a tool by a human operator in order to imitate the demonstrated trajectories. The operator holds the tool in one hand and performs various tasks, such as application of hot glue with a glue gun along various trajectories on a frame, polishing a surface with a grout float, or flattening a cloth with a roller. To learn from such demonstrations, the robot has to identify the 6D pose of the tool. A successful task imitation requires the robot to replicate the trajectory to its own end effector.

Objects and environment setups. The *Imitrob* dataset features three tools (glue gun, grout float, and roller), four demonstrators (subjects S1-S4), and manipulations by the left (LH) and right (RH) hand. The 6D poses of the tools were measured by the HTC Vive (see Sec. 3), and the image data were recorded using two RGB-D cameras, from the front (C1) and right-hand side (C2) viewpoints (see Fig. 2a). While we do not utilize the depth component in this work, it is included in the published dataset, along with the raw data and the code for custom data extraction.

Tasks. The *ImitrobTest* dataset contains six tasks with different tool trajectories: three for glue gun (frame, dense wave, sparse wave), two for grout float (round, sweep), and one for roller (press) (see Fig. 3 Tasks). In addition, the glue gun frame task was recorded in two environments: with only the gluing frame on the table (*NoClutter*, default) and with a clutter of other objects around the gluing

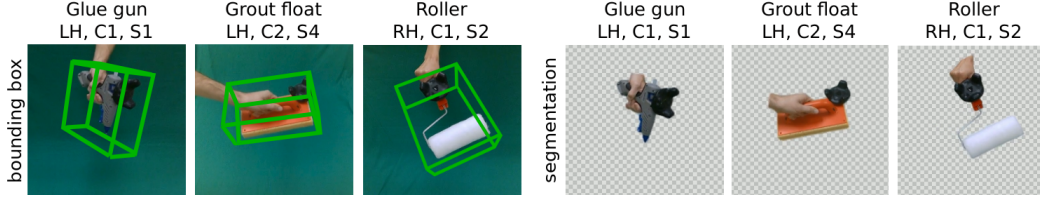


Figure 4: **Example frames from our *ImitrobTrain* dataset.** *Left:* Bounding box of the tool computed from the HTC Vive data. *Right:* Segmentation of the tool and hand computed by the *MaskFBA* method. “LH, C1, S1”, for example, denotes left hand, front camera, and first subject (see Sec. 4.2). The images are cropped to show finer details.

frame (*Clutter*) (see Fig. 3 Clutter). Each task was performed by all four demonstrators (S1-S4) to simulate the variability of tool manipulation by humans. The dataset can thus be used for learning task-specific motions from human demonstration.

Labeling of the data. All RGB-D images collected in the *Imitrob* dataset are accompanied by a reference 6D pose of the tool. The 6D poses were acquired from HTC Vive at 30Hz frequency and interpolated to match the timestamps of the camera frames (see Sec. 3). The calibration of the HTC Vive towards the experimental table and the tool is described in Sec. 3. The *ImitrobTest* dataset contains 45 233, 12 048, and 4 379 annotated frames for glue gun, grout float, and roller, respectively.

Evaluation metrics. We use the following three standard metrics for evaluation of the 6D object pose estimation (see Appendix A.3 for details). 1) The pass rate ADD_t measures the percentage of predictions with ADD lower than a selected threshold t , where ADD [2] is the average distance between the corresponding predicted and reference vertices and centroid of the object 3D bounding box. For a fixed threshold t , a higher ADD_t value indicates a better prediction accuracy of the object bounding box. The ADD metric is useful in imitation learning where we are interested in the absolute error regardless of the size of the manipulated object. For comparison of models trained with and without augmentation (see Sec. 5), we use the ratio of their respective pass rates ADD_t^{ratio} . A higher ADD_t^{ratio} value indicates a bigger benefit of the augmentation. 2) The rotation error E_{rot} measures the angle between the predicted and reference object orientations. A lower E_{rot} value corresponds to a better estimate of the object orientation. 3) The translation error E_{tra} measures the distance between the predicted and reference object positions. A lower E_{tra} value indicates a better localization of the object in space.

4.2 *ImitrobTrain*: Dataset for training

The *ImitrobTrain* dataset (see Fig. 4) is designed for training 6D object pose estimation methods that do not require a 3D model of the object. Instead of creating a complex 3D model, the dataset captures the tools in various orientations to provide sufficient viewpoint variability for 6D object pose training. Each tool was moved randomly in one hand for a short time (20-40 s) to simulate the range of possible 6D poses during manipulation. We designed this process to allow for a time and cost efficient (e.g. without the requirement for manual annotation) extension of the dataset to new tools, as pose estimation methods typically require object-specific training sets. Similarly to the *ImitrobTest* dataset, the *ImitrobTrain* dataset contains the same three tools (glue gun, grout float, and roller), four demonstrators (S1-S4), left and right hand (LH and RH), and two cameras (C1 and C2). In total, there are 48 different tool/camera/hand/demonstrator combinations in the *ImitrobTrain* dataset. In contrast to the *ImitrobTest* dataset, which contains task-specific motions and environments, in the *ImitrobTrain* dataset the tools were randomly rotated in front of a green background, which enables automatic object segmentation for background augmentation (see Appendix A.4). We include the segmented data as well as the reference 6D object pose from HTC Vive in the published *ImitrobTrain* dataset. The *ImitrobTrain* dataset contains 14 584, 12 864, and 11 878 frames for glue gun, grout float, and roller, respectively. The size of the dataset corresponds to the application area of imitation learning in industrial settings, where real data has to be collected from human demonstrators.

Augmentation methods. We provide a collection of data augmentation methods suitable for the *ImitrobTrain* dataset. The augmentation significantly increases the size of the training set and robustness of the trained model to the variability of the test environment. First, we leverage the green

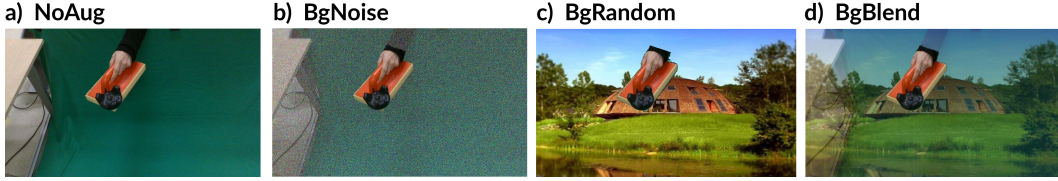


Figure 5: **Augmentation of a frame from the *ImitrobTrain* dataset.** a) Original image (*NoAug*) and background augmentation by b) *BgNoise*, c) *BgRandom* (or *BgAlternate*), and d) *BgBlend*.

Table 1: **Comparison of ADD pass rates for different data augmentation methods** (see Sec.4.2).

ADD ₅	<i>NoAug</i>	<i>BgNoise</i>	<i>BgRandom</i>	<i>BgAlternate</i>	<i>BgBlend</i>
glue gun	17.0	18.9	36.5	45.4	57.8
grout float	45.4	43.6	60.4	71.8	73.9
roller	25.3	26.3	39.8	52.2	48.6
average	29.2	29.6	45.6	56.5	60.1

background to segment the tool and hand by thresholding (*MaskThresholding*), followed by *F*, *B*, Alpha Matting [34] (*MaskFBA*) (see Fig. 4, for details see Appendix A.4). Then we apply a random crop (constrained to keep all vertices of the 3D bounding box inside the image) and horizontal flip, and one of the following background randomization techniques. *BgRandom* replaces the background with a random image [35]. The other three methods keep the original background for 25% of the training images, and for the remaining 75% *BgAlternate* replaces the background with a random image, *BgBlend* blends the background with a random image, and *BgNoise* blends the background with random color noise. In our experiments, the random images were sampled from the miniImageNet [36] dataset of 60 000 images. Fig. 5 shows a training image without augmentation (*NoAug*) and after augmentation by these methods.

5 Exemplar 6D object pose estimation performance

In the following experiments we demonstrate the utility of the *Imitrob* dataset for 6D object pose estimation training and testing. For this purpose we use the DOPE 6D object pose estimator [2] (see Appendix A.5 for the implementation details). We train all models on the *ImitrobTrain* dataset (see Sec. 4.2) and evaluate their performance on the *ImitrobTest* dataset (see Sec. 4.1). We compute the ADD pass rates for $t = 2$ cm (ADD₂), 5 cm (ADD₅) and 10 cm (ADD₁₀) thresholds (for the ADD₂ and ADD₁₀ values, see Appendix A.8, A.9, A.10). First, we present an ablation study to motivate our choice of the data augmentation method. The ablation studies to motivate our choice of the input image resolution and training batch size (see Appendix A.6). Then we focus on the ability of the 6D object pose estimator to generalize to various training/testing setups, including different subjects, front/side camera, left/right hand, and background clutter.

Benefits of data augmentation. Table 1 shows the effect of the background augmentation methods from Sec. 4.2 on the performance of the DOPE 6D object pose estimator. For the object segmentation step, we use the *MaskFBA* method, which outperforms the simple *MaskThresholding* (see Appendix A.7). Real-world images (*BgRandom*, *BgAlternate*, *BgBlend*) clearly outperform color noise (*BgNoise*) as a random background for augmentation. Moreover, it is beneficial to keep the original background for a portion (in our case 25%) of training images (*BgAlternate*, *BgBlend*) rather than to replace the background everywhere (*BgRandom*). The best results were achieved on average by *BgBlend*, which (after the random crop, horizontal flip, and segmentation by the *MaskFBA* method) blends the original background with a random image for 75% of the training images and keeps the original background for the remaining 25% of the training images. The use of *BgBlend* augmentation (ADD₅ = 60.1%) vastly increased the accuracy w.r.t. training without augmentation (*NoAug*, ADD₅ = 29.2%). Thus, in all other experiments, we use the *BgBlend* background augmentation.

Generalization across demonstrators. To be transferable, the 6D pose estimation algorithm should be invariant to the subject that manipulates the tool. We examine the generalization of the DOPE estimator across 4 different subjects (S1-S4) using the following setups: a) AllToSame: train one model on all 4 subjects and test it on each subject (e.g. train on S1-S4 and test on S1); b) All-

Table 2: **Generalization across demonstrators, camera viewpoints, and left/right hand.** Comparison of the 5 cm ADD pass rates for combinations of demonstrators (S1-S4), camera viewpoints (front camera C1, right-hand side camera C2), and holding the tool in the left (LH) or right (RH) hand between training and testing (see Sec.5 for a description of the scenarios). “Same” refers to training and testing on the same camera/hand, “Other” to training on one camera/hand and testing on the other, and “Both” to training on both cameras/hands. “AllToSame” refers to training on all subjects and testing on each of them, “AllToDiff” to training on three subjects and testing on the remaining one, and “SameToSame” to training and testing on the same subject. In the case of subjects, the ADD pass rates are averaged over all four test subjects (S1-S4). The last row shows the averages for models trained without data augmentation (*NoAug*).

ADD ₅	Training camera	Test		Training hand	Test		Subject scenario	Test
		C1	C2		LH	RH		
glue gun	Same	61.6	53.3	Same	60.9	25.6	AllToSame	57.2
	Other	0.2	2.2	Other	8.6	22.8	AllToDiff	52.6
	Both	63.6	50.6	Both	60.8	51.4	SameToSame	32.8
grout float	Same	50.7	66.0	Same	60.7	57.1	AllToSame	77.2
	Other	0.0	1.2	Other	31.1	53.4	AllToDiff	64.1
	Both	78.1	77.3	Both	70.8	83.8	SameToSame	38.8
roller	Same	56.7	37.2	Same	49.9	37.9	AllToSame	41.8
	Other	0.1	0.0	Other	23.3	4.9	AllToDiff	39.1
	Both	66.3	19.1	Both	49.9	35.7	SameToSame	21.8
average	Same	56.3	52.2	Same	57.2	40.2	AllToSame	58.8
	Other	0.1	1.1	Other	21.0	27.0	AllToDiff	52.0
	Both	69.3	49.0	Both	60.5	57.0	SameToSame	31.1
<i>NoAug</i>	<i>Same</i>	28.7	41.8	<i>Same</i>	29.4	22.5	<i>AllToSame</i>	28.9
	<i>Other</i>	0.0	0.8	<i>Other</i>	13.7	18.4	<i>AllToDiff</i>	22.3
	<i>Both</i>	23.5	34.8	<i>Both</i>	31.3	25.6	<i>SameToSame</i>	18.7

ToDiff: train one model for 3 subjects and test it on the remaining one (e.g. train on S1-S3 and test on S4); and c) SameToSame: train one model for each subject and test it on the same subject (e.g. train on S1 and test also on S1). Table 2 averages the model accuracy for each setup across all test subjects (i.e. S1-S4). The AllToSame setup (ADD₅ = 58.8%) outperformed the AllToDiff setup (ADD₅ = 52.0%), which in turn clearly outperformed the SameToSame setup (ADD₅ = 31.1%). Additionally, the augmentation improves the accuracy more for AllToDiff (ADD₅^{ratio} = 2.3) than for the AllToSame (ADD₅^{ratio} = 2.0) and SameToSame (ADD₅^{ratio} = 1.7) setups.

Generalization across camera viewpoints. In this experiment, we study the robustness of the 6D object pose estimator with respect to the camera viewpoint. The *Imitrob* dataset contains one front camera (C1) and one right-hand side camera (C2). Table 2 compares results for the following scenarios: a) Same: training and testing on the same camera; b) Other: training on one camera and testing on the other; c) Both: training on both cameras. For all three tools, the accuracy of using a different camera viewpoint during testing than during training was very low; on average, the results were better for the transfer from C1 to C2 (ADD₅ = 1.1%) than for the transfer from C2 to C1 (ADD₅ = 0.1%). The accuracy was significantly higher when the camera used for testing was included in the training. Whereas the best results for evaluation on C1 were achieved by models trained on both C1 and C2 (Both), for evaluation on C2 the best results were achieved by models trained only on C2 (Same).

Generalization across left/right hand. This experiment explores the generalization of the 6D pose estimator to manipulation of the tool by the left (LH) or right (RH) hand. Table 2 compares the results for the following cases: a) Same: training and testing on the same hand; b) Other: training on one hand and testing on the other; c) Both: training on both hands. While training and testing on the same hand (Same, ADD₅ = 48.7%) is clearly better than on the opposite hand (Other, ADD₅ = 24.0%), using both LH and RH for training further improved the accuracy (Both, ADD₅ = 58.8%). The data augmentation was more beneficial for training on both hands (Both, ADD₅^{ratio} = 2.1) than for training only on the same (Same, ADD₅^{ratio} = 1.7) or opposite hand (Opposite, ADD₅^{ratio} = 1.5).

Robustness to clutter. To explore the generalization of the 6D object pose estimator to clutter in the test data, we compare its performance for the glue gun task frame with only the gluing frame on

Table 3: Performance on different manipulation tasks. 5 cm ADD pass rate (ADD_5) accuracy and average rotation (E_{rot}) and translation (E_{tra}) errors for different tasks with the same tools. Invalid detections (less than 0.5% of frames for each task) were excluded from the computation of E_{rot} and E_{tra} .

Tool	Task	ADD_5 (%)	E_{rot} (deg)	E_{tra} (cm)
glue gun	frame	53.3	11.8	5.0
	densewave	61.9	5.0	3.6
	sparsewave	66.0	5.0	3.4
grout float	round	74.4	3.9	2.7
	sweep	82.7	4.3	2.2
roller	press	50.5	8.7	3.7



Figure 6: Example qualitative results on the *ImitrobTest* dataset. Comparison of the reference bounding box (green) and the bounding box predicted by the 6D object pose estimator DOPE (red) trained on the *ImitrobTrain* dataset. **More qualitative results are available in the supplementary video [6].**

the table (*NoClutter*, default) and with a clutter of other objects around the frame (*Clutter*). While the model trained without data augmentation (*NoAug*) was clearly worse on *Clutter* ($ADD_5 = 4.9$) than on *NoClutter* ($ADD_5 = 22.8$), the use of data augmentation not only clearly improved the performance on both subsets but also increased the accuracy on *Clutter* ($ADD_5 = 61.5$) to the same level as on *NoClutter* ($ADD_5 = 61.8$). The ADD_5^{ratio} improvement ratio was 12.5 for *Clutter*, compared with 2.7 for *NoClutter*, indicating a big benefit of training with data augmentation for 6D object pose estimation in cluttered environment.

Performance on different tasks. Table 3 shows ADD pass rates as well as rotation and translation errors for individual tasks (see Fig. 3). While the 6D pose estimator performed comparably on different tasks of the same tool, the best results were achieved mostly for the grout float. Overall, the average rotation and translation errors were $E_{rot} = 6.5^\circ$ and $E_{tra} = 3.4$ cm, respectively.

Qualitative results. Fig. 6 presents example qualitative results of the DOPE 6D object pose estimator trained on the *ImitrobTrain* dataset using the best data augmentation (i.e. random crop and horizontal flip, segmentation by the *MaskFBA* method, and background randomization by the *BgBlend* method, see Sec. 4.2) and tested on the *ImitrobTest* set. The predicted bounding box is shown in red while the reference bounding box, acquired through the camera-to-tracker and tracker-to-tool calibration (see Sec. 3), is green.

6 Conclusions and lessons learned

In this paper, we address the problem of 6D pose estimation of hand tools manipulated by human demonstrators in an industrial environment from RGB image data. To investigate this problem, we have collected a challenging real-world benchmark video dataset (*Imitrob* dataset) of four human demonstrators performing six manipulation tasks with three different tools recorded from two camera viewpoints (front and side). We performed a broad range of experiments with various parts of the *ImitrobTrain* and *ImitrobTest* datasets using the 6D object pose estimation method DOPE [2] to show the suitability of the *Imitrob* dataset for benchmarking 6D object pose estimation methods as well as to point out the limitations of current methods in this setup. The experiments imply that it is crucial to include in the training data the camera viewpoint used during the inference. Less occlusion of the tool by the hand, when the tool was manipulated by the hand opposite to the side camera, was correlated with higher accuracy of the pose estimator. The performance of models that used the same subject/camera/hand combination in both training and test data was often boosted by adding other demonstrators, camera viewpoint, or the other hand into the training set (see Table 2).

To enhance the training data, we proposed several data augmentation methods that we present together with the dataset. The best results were achieved by the background blending augmentation method *BgBlend* (see Table 1), which increased the generalization capability of the trained models in all setups. To our knowledge, this is the first application of the background blending augmentation,

previously used in image classification [37], in the 6D object pose estimation domain. Although the achieved accuracy of the evaluated method (DOPE) may not be sufficient for some industrial applications (average rotation and translation errors 6.5° and 3.4 cm, respectively, see Table 3), the results are promising and show that the *Imitrob* dataset can be used to benchmark and select 6D object pose estimation methods for various tasks based on the required accuracy. We hope that the presented dataset will trigger further development of 6D object pose estimation methods so that learning by demonstration using only visual information will soon become a reality.

Limitations. The main limitation of our approach is the presence of the tracker, which creates additional occlusions and is likely to be learned as a part of the tool. Nonetheless, this should not affect the main goal of the proposed dataset, i.e. benchmarking of object pose estimation methods on the tool-manipulation tasks, since the tracker is present in both the training and testing sets. For a real application, the HTC Vive tracker could be replaced by a smaller or concealed tracking device, e.g. based on an inertial measuring unit. However, we consider this an engineering problem beyond the scope of this paper. One limitation of the dataset is that the contact between the tool and the environment during each task occurs along a plane (e.g. the top of the gluing frame), which to some degree constrains the poses in the test set. However, these constraints are typical of manipulation tasks with these tools and apply only to the test set, as the tools are moved freely in the training set. In addition, the type of contact with the planar surface differs among the tools: it is a plane in the case of the grout float, a line in the case of the roller, and a point in the case of the glue gun. The orientation of the glue gun, for example, is thus constrained only by the realistic expectation that its tip does not touch the gluing location from the bottom. For other limitations and potential negative societal impact, please see the supplementary material (Appendix B).

Acknowledgment

Jiri Sedlar and Josef Sivic were supported by the European Regional Development Fund under the project IMPACT (reg. no. CZ.02.1.01/0.0/0.0/15_003/0000468). Matus Tuna was supported by project VEGA 1/0796/18 and Inafym project CZ.02.1.01/0.0/0.0/16.019/. Karla Stepanova, Radoslav Skoviera, and Gabriela Sejnova were supported by the Technological Agency of CR under the grant Collaborative workspace of the future (reg. no. FV40319). Gabriela Sejnova was supported by CTU Student Grant Agency (reg. no. SGS21/184/OHK3/3T/37). Radoslav Skoviera, Jan Kristof Behrens, and Robert Babuska were supported by the European Regional Development Fund under the project Robotics for Industry 4.0 (reg. no. CZ.02.1.01/0.0/0.0/15_003/0000470).

References

- [1] Yann Labbé, Justin Carpentier, Mathieu Aubry, and Josef Sivic. CosyPose: Consistent multi-view multi-object 6D pose estimation. In *European Conference on Computer Vision*, pages 574–591. Springer, 2020.
- [2] Jonathan Tremblay, Thang To, Balakumar Sundaralingam, Yu Xiang, Dieter Fox, and Stan Birchfield. Deep object pose estimation for semantic robotic grasping of household objects. *CoRL*, 2018.
- [3] Simon Manschitz, Jens Kober, Michael Gienger, and Jan Peters. Learning movement primitive attractor goals and sequential skills from kinesthetic demonstrations. *Robotics and Autonomous Systems*, 74:97–107, 2015.
- [4] Baris Akgun, Kaushik Subramanian, and Andrea Lockerd Thomaz. Novel interaction strategies for learning from teleoperation. In *2012 AAAI Fall Symposium Series*, 2012.
- [5] M Ehrenmann, R Zollner, S Knoop, and R Dillmann. Sensor fusion approaches for observation of user actions in programming by demonstration. In *Multisensor Fusion and Integration for Intelligent Systems, 2001. MFI 2001. International Conference on*, pages 227–232. IEEE, 2001.
- [6] CIIRC CTU in Prague. Imitrob dataset version 2.0. <http://imitrob.ciirc.cvut.cz/imitrobdataset.php>, 2022.

- [7] CIIRC CTU in Prague. GitHub for Imitrob dataset version 2.0. https://github.com/imitrob/imitrob_dataset_code, 2022.
- [8] Radoslav Skoviera, Karla Stepanova, Michael Tesar, Gabriela Sejnova, Jiri Sedlar, Michal Vavrecka, Robert Babuska, and Josef Sivic. Teaching robots to imitate a human with no on-teacher sensors. What are the key challenges? *arXiv preprint arXiv:1901.08335*, 2019.
- [9] Caner Sahin, Guillermo Garcia-Hernando, Juil Sock, and Tae-Kyun Kim. A review on object pose recovery: From 3D bounding box detectors to full 6D pose estimators. *Image and Vision Computing*, 96, 2020.
- [10] Mario E Munich, Paolo Pirjanian, Enrico Di Bernardo, Luis Goncalves, Niklas Karlsson, and David Lowe. SIFT-ing through features with ViPR. *IEEE Robotics & Automation magazine*, 13(3):72–77, 2006.
- [11] Herbert Bay, Tinne Tuytelaars, and Luc Van Gool. SURF: Speeded up robust features. In *European Conference on Computer Vision (ECCV)*, pages 404–417. Springer, 2006.
- [12] Yu Xiang, Tanner Schmidt, Venkatraman Narayanan, and Dieter Fox. Posecnn: A convolutional neural network for 6d object pose estimation in cluttered scenes. *Robotics: Science and Systems (RSS)*, 2018.
- [13] Chen Wang, Danfei Xu, Yuke Zhu, Roberto Martín-Martín, Cewu Lu, Li Fei-Fei, and Silvio Savarese. DenseFusion: 6D object pose estimation by iterative dense fusion. In *Proceedings of the IEEE/CVF Conference on Computer Vision and Pattern Recognition*, pages 3343–3352, 2019.
- [14] Yi Li, Gu Wang, Xiangyang Ji, Yu Xiang, and Dieter Fox. DeepIM: Deep Iterative Matching for 6D Pose Estimation. In *Proceedings of the European Conference on Computer Vision (ECCV)*, pages 683–698, 2018.
- [15] Sergey Zakharov, Ivan Shugurov, and Slobodan Ilic. DPOD: 6D pose object detector and refiner. In *Proceedings of the IEEE/CVF International Conference on Computer Vision*, pages 1941–1950, 2019.
- [16] Kiru Park, Timothy Patten, and Markus Vincze. Pix2Pose: Pixel-wise coordinate regression of objects for 6D pose estimation. In *Proceedings of the IEEE/CVF International Conference on Computer Vision*, pages 7668–7677, 2019.
- [17] Giorgia Pitteri, Slobodan Ilic, and Vincent Lepetit. CorNet: Generic 3D corners for 6D pose estimation of new objects without retraining. In *Proceedings of the IEEE/CVF International Conference on Computer Vision Workshops*, 2019.
- [18] Tomas Hodan, Daniel Barath, and Jiri Matas. EPOS: Estimating 6D pose of objects with symmetries. In *Proceedings of the IEEE/CVF Conference on Computer Vision and Pattern Recognition*, pages 11703–11712, 2020.
- [19] Yisheng He, Wei Sun, Haibin Huang, Jianran Liu, Haoqiang Fan, and Jian Sun. PVN3D: A deep point-wise 3D keypoints voting network for 6DoF pose estimation. In *Proceedings of the IEEE/CVF Conference on Computer Vision and Pattern Recognition*, pages 11632–11641, 2020.
- [20] Mahdi Rad and Vincent Lepetit. BB8: A scalable, accurate, robust to partial occlusion method for predicting the 3D poses of challenging objects without using depth. In *International Conference on Computer Vision (ICCV)*, 2017.
- [21] Stefan Hinterstoisser, Vincent Lepetit, Slobodan Ilic, Stefan Holzer, Gary Bradski, Kurt Konolige, and Nassir Navab. Model based training, detection and pose estimation of texture-less 3D objects in heavily cluttered scenes. In *Asian Conference on Computer Vision*, pages 548–562. Springer, 2012.
- [22] Eric Brachmann, Alexander Krull, Frank Michel, Stefan Gumhold, Jamie Shotton, and Carsten Rother. Learning 6D object pose estimation using 3D object coordinates. In *European Conference on Computer Vision (ECCV)*, pages 536–551. Springer, 2014.

- [23] Tomáš Hodan, Pavel Haluza, Štěpán Obdržálek, Jiri Matas, Manolis Lourakis, and Xenophon Zabulis. T-LESS: An RGB-D dataset for 6D pose estimation of texture-less objects. In *Applications of Computer Vision (WACV), 2017 IEEE Winter Conference on*, pages 880–888. IEEE, 2017.
- [24] Bertram Drost, Markus Ulrich, Paul Bergmann, Philipp Hartinger, and Carsten Steger. Introducing MVTEC ITODD—a dataset for 3D object recognition in industry. In *Proceedings of the IEEE International Conference on Computer Vision Workshops*, pages 2200–2208, 2017.
- [25] Till Grenzdörffer, Martin Günther, and Joachim Hertzberg. YCB-M: a multi-camera RGB-D Dataset for object recognition and 6DoF pose estimation. In *2020 IEEE International Conference on Robotics and Automation (ICRA)*, pages 3650–3656. IEEE, 2020.
- [26] Pat Marion, Peter R Florence, Lucas Manuelli, and Russ Tedrake. Label fusion: A pipeline for generating ground truth labels for real RGBD data of cluttered scenes. In *2018 IEEE International Conference on Robotics and Automation (ICRA)*, pages 3235–3242. IEEE, 2018.
- [27] Mia Kokic, Danica Kragic, and Jeannette Bohg. Learning task-oriented grasping from human activity datasets. *IEEE Robotics and Automation Letters*, 5(2):3352–3359, 2020.
- [28] Alexander Krull, Frank Michel, Eric Brachmann, Stefan Gumhold, Stephan Ihrke, and Carsten Rother. 6-DoF model based tracking via object coordinate regression. In *Asian Conference on Computer Vision*, pages 384–399. Springer, 2014.
- [29] Morgan Quigley, Ken Conley, Brian Gerkey, Josh Faust, Tully Foote, Jeremy Leibs, Rob Wheeler, Andrew Y Ng, et al. Ros: an open-source robot operating system. In *ICRA workshop on open source software*, volume 3, page 5. Kobe, Japan, 2009.
- [30] G. Bradski. The OpenCV Library. *Dr. Dobb’s Journal of Software Tools*, 2000.
- [31] Hugues Hoppe, Tony DeRose, Tom Duchamp, John McDonald, and Werner Stuetzle. Surface reconstruction from unorganized points. In *Proceedings of the 19th annual conference on Computer graphics and interactive techniques, SIGGRAPH ’92*, page 71–78. Association for Computing Machinery, Jul 1992. ISBN 978-0-89791-479-6. doi: 10.1145/133994.134011. URL <https://doi.org/10.1145/133994.134011>.
- [32] Dawson-Haggerty et al. Trimesh [computer software]. <https://trimsh.org/>, 2019. URL <https://trimsh.org/>.
- [33] Miguel Borges, Andrew Symington, Brian Coltin, Trey Smith, and Rodrigo Ventura. HTC Vive: Analysis and Accuracy Improvement. In *2018 IEEE/RSJ International Conference on Intelligent Robots and Systems (IROS)*, page 2610–2615. IEEE, Oct 2018. ISBN 978-1-5386-8094-0. doi: 10.1109/IROS.2018.8593707. URL <https://ieeexplore.ieee.org/document/8593707/>.
- [34] Marco Forte and François Pitié. *F, B, Alpha Matting*. *arXiv e-prints*, 2020.
- [35] Zongmian Li, Jiri Sedlar, Justin Carpentier, Ivan Laptev, Nicolas Mansard, and Josef Sivic. Estimating 3D Motion and Forces of Human–Object Interactions from Internet Videos. *International Journal of Computer Vision*, pages 1–21, 2022. doi: 10.1007/s11263-021-01540-1.
- [36] Oriol Vinyals, Charles Blundell, Timothy Lillicrap, Daan Wierstra, et al. Matching networks for one shot learning. In *Advances in Neural Information Processing Systems*, pages 3630–3638, 2016.
- [37] Hongyi Zhang, Moustapha Cisse, Yann N. Dauphin, and David Lopez-Paz. mixup: Beyond empirical risk minimization. In *International Conference on Learning Representations (ICLR)*, 2018.
- [38] Olga Sorkine-Hornung and Michael Rabinovich. Least-squares rigid motion using SVD. *Computing*, 1(1):1–5, 2017.
- [39] Diederik P Kingma and Jimmy Ba. Adam: A method for stochastic optimization. *ICLR*, 2015.

Imitrob: Imitation Learning Dataset for Training and Evaluating 6D Object Pose Estimators

Supplementary material

A Appendix - Setup Details and Additional Experimental Results

This appendix provides a detailed description of the sensor setup calibration (see Sec. A.1), including the method for calibration of the HTC Vive tracker to the tool (see Sec. A.2). In Sec. A.3 we provide complete definitions of the used evaluation metrics. The object segmentation methods that we used for background augmentation are described and compared in Sec. A.4. Details about the specific settings of the DOPE [2] method, including the training setup, are given in Sec. A.5.

We also report more detailed experimental results. Sec. A.6 shows the impact of image resolution and batch size on the accuracy of the 6D pose object estimation and Sec. A.7 compares results for augmentation with different object segmentation methods. In Secs. A.8-A.13 we include additional experimental results for the benefits of data augmentation, generalization across demonstrators, camera viewpoints, and left/right hand, robustness to clutter, and performance on different tasks, respectively.

A.1 Sensor setup calibration

To calibrate the HTC Vive coordinate frame O_{htc} (in one of the lighthouses marked as HTC Vive in Fig. 7) to the chessboard coordinate frame O_w , spherical motion patterns centered at different chessboard corners p_w were recorded using an HTC Vive tracker mounted on a pointed metal rod (the rod is shown in Fig. 2b).

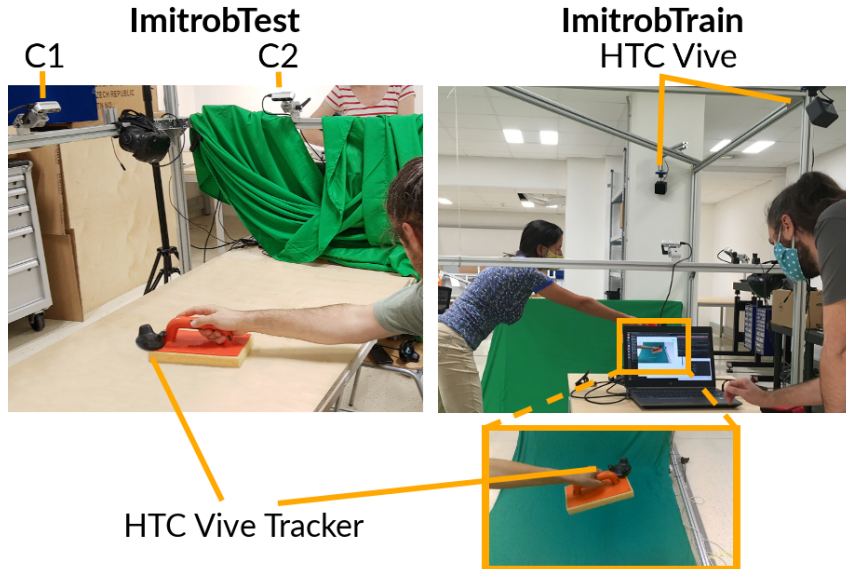


Figure 7: An overview of the experimental setup for collection of *ImitrobTest* and *ImitrobTrain* datasets. The setup consists of two RGB-D cameras (C1 and C2) at 90° angle (front and right-hand side, respectively), two HTC Vive lighthouses, and an HTC Vive tracker attached to the tool.

The sphere center points p_{htc} (relative to O_{htc}) were computed using orthogonal distance regression. The distances of all center points to the common plane found using RANSAC were smaller than 1 mm, i.e. all points lie on the flat plane of the chessboard pattern. The optimal Euclidean transformation H from p_{htc} to p_w (i.e. transformation between O_{htc} and O_w) was found using the SVD algorithm [38]. The average deviation (residual r_{avg}) of the acquired center points from the regular chessboard grid pattern (acquired from the cameras) was below 2 mm for all experiments.

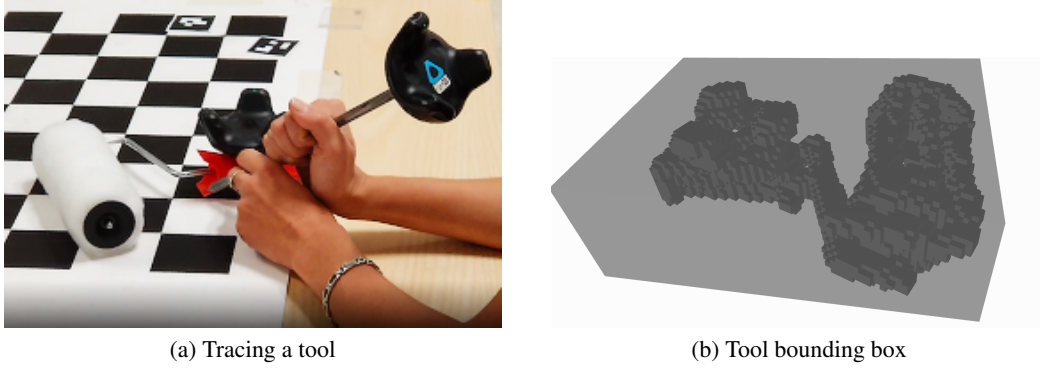


Figure 8: **Calibration of the tool w.r.t. the tracking device.** The tool (roller) surface is traced with a pointing device (see Fig. 8a). The collected data (here 6 364 surface trace points) is used to calculate a voxel grid for the tool (dark grey in Fig. 8b) and the final bounding box (light gray).

The deviation was calculated as

$$r_{\text{avg}} = \frac{1}{2N} \sum_{i=1}^N (\|Hp_{\text{htc}}^i - p_w^i\|_2 + \|H^{-1}p_w^i - p_{\text{htc}}^i\|_2), \quad (1)$$

where N is the number of acquired center points and corresponding points in coordinate frames O_{htc} and O_w have the same index.

The final accuracy of the ground truth poses is also dependent on the ability of the HTC Vive to provide accurate and stable poses of the tracker attached to a tool w.r.t. O_{htc} . The accuracy of HTC Vive in dynamic situations is evaluated in detail in [33].

A.2 HTC Vive Tracker to Tool Calibration

The method presented in this section allows finding a description of the object surface w.r.t. an attached motion tracker that provides reference 6D data. In this paper, it is used to find the bounding boxes of the manipulated objects relative to the tracker, which in turn are used to generate the reference bounding boxes for the *Imitrob* dataset.

Note that the computed bounding boxes do not affect the performance of 6D pose estimators because the training and testing are executed using the same bounding box calibration. The accuracy of the pose annotations is mainly determined by the HTC Vive dynamic accuracy, which was evaluated in [33]. Nonetheless, we look for bounding boxes that 1) contain the object, 2) align with the tracker axis, and 3) are minimal in size. In this way, the bounding boxes can be used to create the segmentation masks provided with the dataset and ensure consistent appearance in different experiments. The tracker attachment was chosen to allow unobstructed handling of the tool and good visibility of the tracker. If possible, the tracker was aligned with the main tool axis. To find the object dimensions relative to the tracker, we traced the tool and tracker surfaces with a pointing device (pointed rod with another HTC Vive tracker) while recording the positions of both trackers (see Fig. 2b). Contour tracing for surface reconstruction was described in [31]. We transform the N recorded pointing tip points into the frame of the tool tracker to obtain a set of measurements $P = \{p_i \in \mathbb{R}^3\}$. The existence of a non-empty set $\hat{P} \subset P$ of outliers makes filtering of the measurements P necessary. Our filtering approach based on measurement density is explained next. For a regular grid V within the axis-aligned bounding box of the traced volume, we calculate a measurement density d_i as the number of measurements closer than a threshold δ at each grid vertex $v_i \in V$:

$$d_i = \sum_{p_i \in \Gamma} \begin{cases} 0 & \text{if } \|p_i - v_i\|_2 > \delta \\ 1 & \text{if } \|p_i - v_i\|_2 \leq \delta, \end{cases} \quad (2)$$

where Γ is a subset of the set of measured points P . We consider the voxel centered at grid vertex v_i to be part of the object surface if the density of measurements d_i at the given grid cell is larger than a threshold ζ , i.e. $d_i \geq \zeta$. To approximate Eq. (2) for the purpose of comparing it with the threshold

ζ , we use a k - d *Tree* to efficiently organize the measurement points $p_i \in P$ and query it for the $\zeta + 1$ nearest neighbors P_i for each grid vertex v_i with a cut-off distance of $\delta + \epsilon$. We evaluate Eq. (2) for $\Gamma = P_i$ to decide if v_i is part of the object’s surface. In short, we decide for each grid point whether it is part of the tool’s surface by evaluating how many measurements are present in its vicinity. For efficiency, we check only just enough nearest neighbors to decide if the threshold was reached.

From this, we create a voxel grid with the dimensions of the object, on which we calculate a minimal bounding box using the trimesh library [32]. To find instead the smallest bounding box that is aligned with the tracker’s z -axis (second bounding box property), we rotate the occupied voxels in 0.1° steps around the z -axis and record the volume of each axis-aligned bounding box. The rotation with the smallest volume is then used. In this work, we used $\delta = 0.01m$ and a resolution of 200 grid points per meter. Fig. 2c visualizes the resulting voxel grid (dark gray) and the bounding box (light gray) for the roller.

A.3 Definitions of evaluation metrics

ADD pass rate. The ADD [2] is defined as the average Euclidean distance between the corresponding predicted and reference vertices and centroid of the object 3D bounding box. The pass rate ADD_t is defined as the percentage of model predictions m^p with ADD lower than a selected threshold t :

$$ADD_t = \frac{\# m^p[\text{where } ADD(m^p) < t]}{\# m^p} \cdot 100\% . \quad (3)$$

The ADD_t^{ratio} is defined as

$$ADD_t^{\text{ratio}} = \frac{ADD_t^{\text{aug}}}{ADD_t^{\text{noaug}}} , \quad (4)$$

where ADD_t^{aug} and ADD_t^{noaug} correspond to training with and without augmentation, respectively.

Rotation error. The rotation error measures the angle between the predicted (R_{pre}) and reference (R_{ref}) object orientations using the rotation part of the rotation-translation matrix:

$$E_{\text{rot}} = \arccos \left(\frac{\text{trace}(R_{\text{pre}}^{-1} R_{\text{ref}}) - 1}{2} \right) . \quad (5)$$

Translation error. The translation error measures the Euclidean distance between the predicted (t_{pre}) and reference (t_{ref}) translation vectors:

$$E_{\text{tra}} = \|t_{\text{pre}} - t_{\text{ref}}\|_2 . \quad (6)$$



Figure 9: **Segmentation of a frame from the *ImitrobTrain* dataset.** a) Original image (*NoAug*) and segmentation of the tool and hand by b) *MaskThresholding* and c) *MaskFBA* (see Sec. A.4).

A.4 Object segmentation methods for background augmentation

In order to augment the image background, we need to segment the shape of the object. Because we work with hand-held tools that are heavily occluded by the hand, we segment both the tool and the hand. We leverage the green background in the *ImitrobTrain* dataset to segment the image by thresholding. To remove the rest of the arm, we crop the segmentation mask by the convex hull of the tool 3D bounding box vertices projected into the 2D image. The result is a binary mask of the tool

and hand (*MaskThresholding*, see Fig. 9b). We enhance the segmentation by F , B , Alpha Matting [34], which estimates also the foreground opacity and color along the boundaries. The output is an RGBA image with opaque foreground, transparent background, and smooth boundaries between them (*MaskFBA*, see Fig. 9c).

Table 4: **Impact of input image resolution and batch size on DOPE 6D object pose accuracy** (see Sec. A.6). ADD pass rates achieved by models trained using the original resolution of *Imitrob* frames (848×480 pixels) with batch size 8 and the images downsized by a factor of two (424×240 pixels) with batch size 16.

ADD _t threshold t	848×480 pixels			424×240 pixels		
	2 cm	5 cm	10 cm	2 cm	5 cm	10 cm
glue gun	7.4	49.8	75.6	9.9	57.8	79.8
grout float	12.5	75.6	93.0	9.7	73.9	97.7
roller	4.5	40.3	67.4	4.3	48.6	84.9
average	8.1	55.2	78.7	8.0	60.1	87.5

A.5 DOPE estimator parameters

We estimate the 6D object pose by the DOPE method [2] in each frame and concatenate the frame predictions into a complete trajectory. Since we focus our evaluation on pose estimation in separate images, we do not post-process the individual frame predictions with any temporal or dynamic model. Our implementation of the DOPE method was based on the referenced PyTorch implementation by [2]. We trained our models on Nvidia 1080Ti and Nvidia V100 GPUs for 10 epochs using the ADAM optimizer [39], learning rate 0.0001, and batch size 16. To be able to train with this batch size, we downsized the input image dimensions by half to 424×240 pixels, which decreased the training time without a negative impact on the accuracy (see Sec. A.6 for the corresponding ablation study). The ground truth belief maps we used for the DOPE training contain a 2D Gaussian with 2-pixel standard deviation and 2-pixel radius at the bounding box vertices and centroid. In all experiments, we train on subsets of the *ImitrobTrain* dataset and test on subsets of the *ImitrobTest* dataset.

A.6 Impact of image resolution and batch size

We explore the impact of downsizing the input images and increasing the batch size on the quality of the 6D object pose estimation by DOPE. Table 4 presents a comparison of ADD pass rates for the original (848×480 pixels, batch size 8) and downsized (424×240 pixels, batch size 16) frames. While the similarity in performance for the 2 cm threshold could be attributed to a trade-off between the larger batch size and loss of detail, the increased batch size clearly improved the accuracy for the 5 cm and 10 cm thresholds. Therefore, we use the 424×240 pixel resolution and batch size 16 for all other experiments.

A.7 Comparison of object segmentation methods

Table 5 compares the ADD pass rates for the *MaskThresholding* and *MaskFBA* object segmentation methods (see Sec. A.4). Because *MaskFBA* outperforms *MaskThresholding* on average for all three thresholds, we use *MaskFBA* for object segmentation in all other experiments.

Table 5: **Comparison of object segmentation methods** (see Sec. A.7). ADD pass rates achieved by models trained using different object segmentation methods (see Sec. A.4) for data augmentation.

ADD _t threshold t	<i>MaskThresholding</i>			<i>MaskFBA</i>		
	2 cm	5 cm	10 cm	2 cm	5 cm	10 cm
glue gun	9.4	57.4	78.4	10.7	60.2	80.6
grout float	10.7	77.8	97.1	10.5	73.0	97.3
roller	4.3	41.2	81.3	4.3	50.5	86.3
average	8.1	58.8	85.6	8.5	61.2	88.1

Table 6: **Comparison of data augmentation methods** (see Sec. A.8). ADD pass rates achieved by models trained with different data augmentation methods (see Sec. 5).

ADD _t threshold <i>t</i>	<i>NoAug</i>			<i>BgNoise</i>			<i>BgRandom</i>			<i>BgAlternate</i>			<i>BgBlend</i>		
	2 cm	5 cm	10 cm	2 cm	5 cm	10 cm	2 cm	5 cm	10 cm	2 cm	5 cm	10 cm	2 cm	5 cm	10 cm
glue gun	1.1	17.0	36.3	1.1	18.9	41.7	6.7	36.5	53.4	5.6	45.4	72.2	9.9	57.8	79.8
grout float	5.3	45.4	80.3	3.3	43.6	86.1	7.7	60.4	84.2	9.6	71.8	95.8	9.7	73.9	97.7
roller	3.4	25.3	56.6	3.8	26.3	52.9	2.9	39.8	85.5	6.3	52.2	85.6	4.3	48.6	84.9
average	3.3	29.2	57.8	2.7	29.6	60.2	5.8	45.6	74.4	7.2	56.5	84.5	8.0	60.1	87.5

Table 7: **Generalization across demonstrators** (see Sec. A.9). Comparison of ADD pass rates for various combinations of the four demonstrators (S1-S4) between training and testing. “AllToSame” refers to training one model for all subjects, “AllToDiff” to training on three subjects and testing on the remaining one, and “SameToSame” to training and testing on the same subject. The ADD pass rates are averaged across all test subjects (i.e. S1-S4). The last row shows the average for models trained without data augmentation (*NoAug*).

ADD _t threshold <i>t</i>	AllToSame			AllToDiff			SameToSame		
	2 cm	5 cm	10 cm	2 cm	5 cm	10 cm	2 cm	5 cm	10 cm
glue gun	10.1	57.2	80.1	6.2	52.6	78.2	3.4	32.8	69.4
grout float	9.5	77.2	97.5	6.0	64.1	95.3	1.8	38.8	81.6
roller	3.9	41.8	78.1	4.5	39.1	77.3	0.7	21.8	53.8
average	7.9	58.8	85.2	5.6	52.0	83.6	2.0	31.1	68.3
<i>NoAug</i>	3.1	28.9	57.7	1.9	22.3	52.3	1.2	18.7	51.6

A.8 Benefits of data augmentation

Table 6 shows 2 cm, 5 cm, and 10 cm ADD pass rates for the DOPE estimator using different background augmentation methods from Sec. 4.2 of the paper. For all three thresholds, the best average ADD pass rates were achieved by the *BgBlend* augmentation. $ADD_2^{\text{ratio}} = 2.4$, $ADD_5^{\text{ratio}} = 2.1$, and $ADD_{10}^{\text{ratio}} = 1.5$ values for *BgBlend* indicate a big improvement in accuracy w.r.t. training without augmentation (*NoAug*).

A.9 Generalization across demonstrators

Table 7 shows the 2 cm, 5 cm, and 10 cm ADD pass rates for the DOPE 6D object pose estimator for various combinations of the demonstrators between training and testing (see Sec. 5 for a detailed description of the scenarios).

A.10 Generalization across camera viewpoints

Table 8 shows the 2 cm, 5 cm, and 10 cm ADD pass rates for the DOPE 6D object pose estimator for various combinations of the camera viewpoints between training and testing (see Sec. 5 for a detailed description of the scenarios).

A.11 Generalization across left/right hand

Table 9 shows the 2 cm, 5 cm, and 10 cm ADD pass rates for the DOPE 6D object pose estimator for various combinations of the left/right hand between training and testing (see Sec. 5 for a detailed description of the scenarios).

A.12 Robustness to clutter

Table 10 shows the 2 cm, 5 cm, and 10 cm ADD pass rates for the DOPE 6D object pose estimator for the presence/absence of clutter in the test environment (see Sec. 5 for a detailed description of the scenarios).

Table 8: **Generalization across camera viewpoints** (see Sec. A.10). Comparison of ADD pass rates for combinations of camera viewpoints (front camera C1, right-hand side camera C2) between training and testing. “Same” refers to training and testing on the same camera, “Other” to training on one camera and testing on the other, and “Both” to training on both cameras. The last row shows the average values for models trained without data augmentation (*NoAug*).

ADD _t threshold <i>t</i>	Training camera	Test C1			Test C2		
		2 cm	5 cm	10 cm	2 cm	5 cm	10 cm
glue gun	Same	8.7	61.6	84.6	5.8	53.3	82.6
	Other	0.0	0.2	1.8	0.1	2.2	12.0
	Both	13.7	63.6	83.4	6.3	50.6	75.0
grout float	Same	2.4	50.7	90.1	6.7	66.0	96.2
	Other	0.0	0.0	0.1	0.0	1.2	21.5
	Both	13.2	78.1	97.8	6.7	77.3	97.3
roller	Same	5.9	56.7	80.9	0.4	37.2	89.0
	Other	0.0	0.1	1.2	0.0	0.0	0.0
	Both	8.2	66.3	85.8	0.0	19.1	72.8
average	Same	5.7	56.3	85.2	4.3	52.2	89.3
	Other	0.0	0.1	1.0	0.0	1.1	11.2
	Both	11.7	69.3	89.0	4.4	49.0	81.7
<i>NoAug</i>	<i>Same</i>	<i>1.7</i>	<i>28.7</i>	<i>66.0</i>	<i>3.2</i>	<i>41.8</i>	<i>74.3</i>
	<i>Other</i>	<i>0.0</i>	<i>0.0</i>	<i>0.6</i>	<i>0.0</i>	<i>0.8</i>	<i>8.0</i>
	<i>Both</i>	<i>3.0</i>	<i>23.5</i>	<i>54.3</i>	<i>3.5</i>	<i>34.8</i>	<i>61.1</i>

Table 9: **Generalization across left and right hand** (see Sec. A.11). Comparison of ADD pass rates for combinations of holding the tool in the left (LH) or right (RH) hand between training and testing. “Same” refers to training and testing on the same hand, “Other” to training on one hand and testing on the other, and “Both” to training on both left and right hand. The last row shows the average values for models trained without data augmentation (*NoAug*).

ADD _t threshold <i>t</i>	Training hand	Test LH			Test RH		
		2 cm	5 cm	10 cm	2 cm	5 cm	10 cm
glue gun	Same	5.6	60.9	77.6	1.8	25.6	56.9
	Other	0.7	8.6	25.0	1.1	22.8	54.8
	Both	8.3	60.8	87.0	8.2	51.4	74.9
grout float	Same	3.2	60.7	95.3	3.4	57.1	93.7
	Other	1.2	31.1	74.5	2.3	53.4	81.2
	Both	7.9	70.8	97.8	11.0	83.8	98.3
roller	Same	5.9	49.9	83.0	1.6	37.9	73.4
	Other	0.8	23.3	45.1	0.3	4.9	22.7
	Both	9.4	49.9	89.3	4.9	35.7	75.4
average	Same	4.9	57.2	85.3	2.3	40.2	74.6
	Other	0.9	21.0	48.2	1.2	27.0	52.9
	Both	8.5	60.5	91.4	8.0	57.0	82.8
<i>NoAug</i>	<i>Same</i>	<i>1.9</i>	<i>29.4</i>	<i>57.1</i>	<i>1.5</i>	<i>22.5</i>	<i>51.9</i>
	<i>Other</i>	<i>0.9</i>	<i>13.7</i>	<i>35.0</i>	<i>0.8</i>	<i>18.4</i>	<i>47.6</i>
	<i>Both</i>	<i>4.0</i>	<i>31.3</i>	<i>58.4</i>	<i>2.0</i>	<i>25.6</i>	<i>52.6</i>

Table 10: **Robustness to clutter** (see Sec. A.12). Comparison of ADD pass rates for glue gun task frame tested on a table with only the gluing frame (*NoClutter*) and with a clutter of other objects around the frame (*Clutter*). The bottom row shows results for a model trained without data augmentation (*NoAug*).

ADD _t threshold <i>t</i>	<i>NoClutter</i>			<i>Clutter</i>		
	2 cm	5 cm	10 cm	2 cm	5 cm	10 cm
glue gun (frame)	8.6	61.8	90.1	11.0	61.5	83.7
<i>NoAug</i>	<i>1.7</i>	<i>22.8</i>	<i>47.7</i>	<i>0.3</i>	<i>4.9</i>	<i>19.8</i>

Table 11: **Performance on different manipulation tasks** (see Sec. A.13). ADD pass rate (ADD_t) accuracy and average rotation (E_{rot}) and translation (E_{tra}) errors for different tasks with the same tools. Invalid detections (less than 0.5% of frames for each task) were excluded from the computation of E_{rot} and E_{tra} .

Tool	Task	ADD _t (%)			E_{rot} (deg)	E_{tra} (cm)
		2 cm	5 cm	10 cm		
glue gun	frame	8.0	53.3	77.1	11.8	5.0
	densewave	10.6	61.9	88.6	5.0	3.6
	sparsewave	8.3	66.0	91.0	5.0	3.4
grout float	round	9.2	74.4	98.7	3.9	2.7
	sweep	9.3	82.7	98.1	4.3	2.2
roller	press	4.3	50.5	86.3	8.7	3.7

A.13 Performance on different tasks

Table 11 shows the 2 cm, 5 cm, and 10 cm ADD pass rates as well as the rotation and translation errors (see Sec. A.3) for the individual tasks in the *ImitrobTest* dataset.

B Limitations and potential societal impact

We describe the main technical limitation of our approach, i.e. the need to mount the tracker on the object, in Sec. 6. Further limitations include biases of the collected data, which might limit the usability and possibly lead to incorrect use by less experienced users. For example, since all our demonstrators have light skin, the results for demonstrators with dark skin may differ. On the other hand, our dataset is gender-balanced, with two female and two male demonstrators.

Potential negative societal impacts might include the loss of jobs if imitation learning of hand-held tools succeeds and becomes widely used. On the other hand, this work could lead to automation of unhealthy jobs (e.g. manipulation with heavy objects, repetitive movements, etc.) and enable workers to transit to more creative and enjoyable positions.

C Dataset documentation and intended uses

Dataset documentation. The *Imitrob* dataset documentation, metadata and download instructions are available at: <http://imitrob.ciirc.cvut.cz/imitrobdataset.php>

Supplementary code. The GitHub repository for the supplementary code (including example usage of the DOPE [2] method) is at: https://github.com/imitrob/imitrob_dataset_code

Intended uses. The dataset is primarily intended for benchmarking 6D pose estimation methods in manipulation tasks with hand-held objects and evaluating their ability to generalize with respect to various conditions. It can be also used to evaluate the effect of different data augmentation methods. Another usage is the methodology for data acquisition and 6D pose estimator training for new tools and tasks and a guideline for collecting more extensive datasets and benchmarking 6D object pose estimators on various tasks with hand-held tools, e.g. in imitation learning, grasping, virtual or augmented reality, etc. In general, we hope that the presented dataset will trigger further development of 6D object pose estimation methods and their usage in various industrial tasks based on the required accuracy.

Author statement. We bear all responsibility in case of violation of right in using our dataset or code. We confirm that we used all the existing assets in accordance to their license.

D Hosting, licensing, and maintainance plan

Hosting. The *Imitrob* dataset is hosted on our in-house servers, which are managed by our dedicated IT department. The dataset and source code are publicly available. The dataset website (<http://imitrob.ciirc.cvut.cz/imitrobdataset.php>) describes the dataset and provides download links. The dataset will be assigned a DOI after the review process. The source code is hosted on https://github.com/imitrob/imitrob_dataset_code.

Maintainance. The authors will provide important bug fixes to the community as commits to the GitHub repository. The dataset webpage will summarize changes to the code and the dataset. In the unlikely case that our in-house data center stops operating, we will migrate the dataset to another hosting and announce the new links in the GitHub repository.

Licensing. The provided dataset and supplementary code are copyrighted by us and published under the CC BY-NC-SA 4.0 license². To use the code or the dataset, the original work has to be attributed, as specified by the authors on the dataset or code repository websites.

Contributions. Contributions to the dataset and supplementary code are welcome and contributors should contact the authors.

Contact. The contact e-mail address of the manager of the dataset: karla.stepanova@cvut.cz.

²<https://creativecommons.org/licenses/by-nc-sa/4.0/>

E Datasheet for dataset *Imitrob*

Questions from the Datasheets for Datasets (<https://arxiv.org/abs/1803.09010>) paper, v7.

E.1 Motivation

For what purpose was the dataset created?

The *Imitrob* dataset was created with the aim to enable imitation learning of manipulation tasks purely from visual observations. This includes the ability to recognize 6D pose of the hand-held objects. Current methods are typically trained and tested in different conditions than this kind of tasks, so it is very difficult to estimate how they will perform in manipulation tasks with hand-held tools. As expected, the tested methods showed quite low accuracy in the case of the manipulation with hand-held tools, especially when generalization to new users, camera viewpoints, or tasks was needed. This motivated the creation of a new dataset, which would enable benchmarking of these methods.

Who created the dataset (e.g., which team, research group) and on behalf of which entity (e.g., company, institution, organization)?

The dataset was created by Jiri Sedlar, Karla Stepanova, Radoslav Skoviera, Gabriela Sejnova, Jan K. Behrens, and Josef Sivic within CIIRC CTU in Prague (Imitation learning centre <http://imitrob.ciirc.cvut.cz>) in collaboration with Matus Tuna from Comenius University in Bratislava and Robert Babuska from TU Delft.

Who funded the creation of the dataset?

Jiri Sedlar and Josef Sivic were supported by the European Regional Development Fund under the project IMPACT (reg. no. CZ.02.1.01/0.0/0.0/15_003/0000468). Matus Tuna was supported by project VEGA 1/0796/18 and Inafym project CZ.02.1.01/0.0/0.0/16.019/. Karla Stepanova, Radoslav Skoviera, and Gabriela Sejnova were supported by the Technological Agency of CR under the grant Collaborative workspace of the future (reg. no. FV40319). Gabriela Sejnova was supported by CTU Student Grant Agency (reg. no. SGS21/184/OHK3/3T/37). Radoslav Skoviera, Jan Kristof Behrens, and Robert Babuska were supported by the European Regional Development Fund under the project Robotics for Industry 4.0 (reg. no. CZ.02.1.01/0.0/0.0/15_003/0000470).

E.2 Composition

What do the instances that comprise the dataset represent (e.g., documents, photos, people, countries)?

The dataset consists of RGB-D images extracted from 104 video sequences, accompanied by 6D annotation. The videos capture simple manipulation tasks with 3 hand-held tools (glue gun, grout float, and roller) such as applying glue along a given trajectory, polishing a surface, or flattening a cloth.

How many instances are there in total (of each type, if appropriate)?

The *Imitrob* dataset contains images extracted from 104 video sequences (56 in the *ImitrobTest* dataset and 48 in the *ImitrobTrain* dataset) of hand-held tool manipulations. The *ImitrobTest* component of the dataset contains 61 660 images and the *ImitrobTrain* component contains 39 326 images.

Does the dataset contain all possible instances or is it a sample (not necessarily random) of instances from a larger set?

The dataset contains all the possible instances.

What data does each instance consist of?

Each video frame contains the following data:

- 6D pose of the recorded tool (6DOF/*.json)

- 2D image coordinates of the tool 3D bounding box vertices and centroid (BBox/*.json)
- depth image (Depth/*.png)
- RGB image (Image/*.png)

In addition, each frame of the *ImitrobTrain* dataset also contains:

- binary mask of the segmented tool and hand (Mask_thresholding/*.png)
- RGB image with the segmented tool and hand opaque and the background transparent (Mask/*.png)

Each video sequence in the *Imitrob* dataset contains:

- 3D coordinates of the tool bounding box vertices and centroid with respect to the HTC Vive Tracker (BB_in_tracker) and intrinsic camera matrices for cameras C1 (K_C1) and C2 (K_C2) (parameters.json)

The training/test component, tool, task, subject, camera, left/right hand or presence/absence of clutter are identified in the name of the video sequence folder.

Is there a label or target associated with each instance?

Yes, each image is annotated with the 6D pose of the tool as well as the video sequence labels, including the identifier of the training/test component, tool, task, subject, camera viewpoint, left/right hand, or presence/absence of clutter.

Is any information missing from individual instances?

The 6D pose for individual data frames was interpolated. When the time difference between consecutive HTC Vive frames was longer than 100 ms, the corresponding camera images were discarded to ensure sufficient accuracy of the ground truth data.

Otherwise no information is missing and the data is complete.

Are relationships between individual instances made explicit (e.g., users' movie ratings, social network links)?

Yes, the relationships are fully identified by the video sequence labels (see above) and the position of the frame in the sequence.

Are there recommended data splits (e.g., training, development/validation, testing)?

We explicitly state the data splits used for training and testing of the 6D pose estimator. The training set is an (augmented) subset of the *ImitrobTrain* dataset, and the test set is a subset of the *ImitrobTest* dataset.

Are there any errors, sources of noise, or redundancies in the dataset?

Sources of noise include the calibration of the cameras and the HTC Vive controllers and the synchronization between the HTC Vive and the cameras (the HTC Vive data were interpolated to the closest camera frame and if the distance between 2 consecutive frames was longer than 100 ms, the corresponding camera images were discarded to ensure sufficiently accurate ground truth data).

Is the dataset self-contained, or does it link to or otherwise rely on external resources (e.g., websites, tweets, other datasets)?

Both the dataset and the supplementary code are self-contained.

Does the dataset contain data that might be considered confidential (e.g., data that is protected by legal privilege or by doctor-patient confidentiality, data that includes the content of individuals' non-public communications)?

N/A.

Does the dataset contain data that, if viewed directly, might be offensive, insulting, threatening, or might otherwise cause anxiety?

N/A.

Does the dataset relate to people?

N/A.

Does the dataset identify any subpopulations (e.g., by age, gender)?

N/A.

Is it possible to identify individuals (i.e., one or more natural persons), either directly or indirectly (i.e., in combination with other data) from the dataset?

N/A.

Does the dataset contain data that might be considered sensitive in any way (e.g., data that reveals racial or ethnic origins, sexual orientations, religious beliefs, political opinions or union memberships, or locations; financial or health data; biometric or genetic data; forms of government identification, such as social security numbers; criminal history)?

N/A.

Any other comments?

N/A.

E.3 Collection process

How was the data associated with each instance acquired?

The directly observable data (RGB-D images) were synchronized with observable HTC Vive data. The parameters of each video sequence setup (such as the tool, task, subject, camera viewpoint, left/right hand, or presence/absence of clutter) were manually annotated and associated with the corresponding data.

What mechanisms or procedures were used to collect the data (e.g., hardware apparatus or sensor, manual human curation, software program, software API)?

The visual part of the dataset was collected by two RGB-D cameras, specifically Intel RealSense D-435. The resolution of both RGB and depth images was set to 848x480 and they were recorded at 60 FPS. The 6D pose information was recorded using HTC Vive VR system in standard configuration. An HTC Vive tracker was mounted to the tools to acquire their pose. The cameras and HTC Vive system were calibrated towards a common coordinate system. The calibration of the camera and HTC Vive was validated by the average distances of associated points using a checkerboard pattern. The whole acquisition system was implemented via the Robot Operating System, using Python as the main programming language.

If the dataset is a sample from a larger set, what was the sampling strategy (e.g., deterministic, probabilistic with specific sampling probabilities)?

N/A.

Who was involved in the data collection process (e.g., students, crowdworkers, contractors) and how were they compensated (e.g., how much were crowdworkers paid)?

Only the authors were involved in the collection process.

Over what timeframe was the data collected?

The data was collected over the timeframe of 2 months (1-2/2021).

Were any ethical review processes conducted (e.g., by an institutional review board)?

N/A.

Does the dataset relate to people?

N/A.

E.4 Preprocessing/cleaning/labeling

Was any preprocessing/cleaning/labeling of the data done (e.g., discretization or bucketing, tokenization, part-of-speech tagging, SIFT feature extraction, removal of instances, processing of missing values)?

The data were originally recorded as ROS bag files, from which the individual data instances were extracted, synchronized, interpolated, and saved to separate folders.

For the *ImitrobTrain* dataset, the masks were created by automatic segmentation of the RGB images.

Was the “raw” data saved in addition to the preprocessed/cleaned/labeled data (e.g., to support unanticipated future uses)?

The original bag files are saved on our internal data storage, but are too big to be easily shareable.

Is the software used to preprocess/clean/label the instances available?

No, we don't provide the raw data and thus neither the code to process it. Dataset manipulation tools (for the already preprocessed and labeled data) are available on the supplementary code GitHub page: https://github.com/imitrob/imitrob_dataset_code.

E.5 Uses

Has the dataset been used for any tasks already?

This is the first use of the dataset.

Is there a repository that links to any or all papers or systems that use the dataset?

There are no papers that use our dataset, yet. Future uses will be added to the dataset/code website.

What (other) tasks could the dataset be used for?

The dataset is primarily intended for benchmarking 6D pose estimation methods in manipulation tasks with hand-held objects and evaluating their ability to generalize with respect to various conditions. It can be also used to evaluate the effect of different data augmentation methods. Another usage is the methodology for data acquisition and 6D pose estimator training for new tools and tasks and a guideline for collecting more extensive datasets and benchmarking 6D object pose estimators on various tasks with hand-held tools, e.g. in imitation learning, grasping, virtual or augmented reality, etc. In general, we hope that the presented dataset will trigger further development of 6D object pose estimation methods and their usage in various industrial tasks based on the required accuracy.

Is there anything about the composition of the dataset or the way it was collected and preprocessed/cleaned/labeled that might impact future uses?

N/A.

Are there tasks for which the dataset should not be used?

N/A.

E.6 Distribution

Will the dataset be distributed to third parties outside of the entity (e.g., company, institution, organization) on behalf of which the dataset was created?

N/A.

How will the dataset will be distributed (e.g., tarball on website, API, GitHub)?

The dataset is available on the dataset website: <http://imitrob.ciirc.cvut.cz/imitrobdataset.php>

When will the dataset be distributed?

In 2022.

Will the dataset be distributed under a copyright or other intellectual property (IP) license, and/or under applicable terms of use (ToU)?

The newly provided datasets and benchmarks are copyrighted by us and published under the CC BY-NC-SA 4.0 license³.

Have any third parties imposed IP-based or other restrictions on the data associated with the instances?

N/A.

Do any export controls or other regulatory restrictions apply to the dataset or to individual instances?

N/A.

E.7 Maintenance

Who is supporting/hosting/maintaining the dataset?

Karla Stepanova at CIIRC CTU in Prague.

How can the owner/curator/manager of the dataset be contacted (e.g., email address)?

Contact e-mail address: karla.stepanova@cvut.cz

Is there an erratum?

Any updates to the code will be visible as commits in the GitHub repository. The dataset website will summarize all changes to the code and the dataset.

Will the dataset be updated (e.g., to correct labeling errors, add new instances, delete instances)?

Any updates to the code will be visible as commits in the GitHub repository. The dataset website will summarize all changes to the code and the dataset.

³<https://creativecommons.org/licenses/by-nc-sa/4.0/>

If the dataset relates to people, are there applicable limits on the retention of the data associated with the instances (e.g., were individuals in question told that their data would be retained for a fixed period of time and then deleted)?

N/A

Will older versions of the dataset continue to be supported/hosted/maintained?

N/A.

If others want to extend/augment/build on/contribute to the dataset, is there a mechanism for them to do so?

Yes, contributions to the dataset are welcome. Please contact the maintainer of the dataset via e-mail (see above).